

# Faster Molecular Dynamics with Neural Network Potentials via Distilled Multiple Time-Stepping and Non-Conservative Forces

Nicolaï Gouraud<sup>1</sup>, Côme Cattin<sup>2</sup>, Thomas Plé<sup>2,\*</sup>, Olivier Adjoua<sup>2</sup>, Louis Lagardère<sup>1,2</sup>, and Jean-Philip Piquemal<sup>1,2,\*</sup>

<sup>1</sup>Qubit Pharmaceuticals, Advanced Research Department, 75014 Paris, France

<sup>2</sup>Sorbonne Université, Laboratoire de Chimie Théorique, UMR 7616 CNRS, 75005 Paris, France

\*Contact authors: [thomas.ple@sorbonne-universite.fr](mailto:thomas.ple@sorbonne-universite.fr),  
[jean-philip.piquemal@sorbonne-universite.fr](mailto:jean-philip.piquemal@sorbonne-universite.fr)

February 17, 2026

## Abstract

Following our previous work (J. Phys. Chem. Lett., 2026, 17, 5, 1288–1295), we propose the DMTS-NC approach, a distilled multi-time-step (DMTS) strategy using non conservative (NC) forces to further accelerate atomistic molecular dynamics simulations using foundation neural network models. There, a dual-level reversible reference system propagator algorithm (RESPA) formalism couples a target accurate conservative potential to a simplified distilled representation optimized for the production of non-conservative forces. Despite being non-conservative, the distilled architecture is designed to enforce key physical priors, such as equivariance under rotation and cancellation of atomic force components. These choices facilitate the distillation process and therefore improve drastically the robustness of simulation, significantly limiting the “holes” in the simpler potential, thus achieving excellent agreement with the forces data. Overall, the DMTS-NC scheme is found to be more stable and efficient than its conservative counterpart with additional speedups reaching 15-30% over DMTS. Requiring no fine-tuning steps, it is easier to implement and can be pushed to the limit of the systems physical resonances to maintain accuracy while providing maximum efficiency. As for DMTS, DMTS-NC is applicable to any neural network potential.

## 1 Introduction

Molecular dynamics (MD) [1, 2] is a popular numerical tool aimed at inferring properties of matter from computer simulations at the atomistic level. With the steady development of efficient algorithms and computational power, “in silico” methods enable the simulation of increasingly complex systems with high accuracy, driving a variety of scientific applications in biology, chemistry, drug design and material sciences [3]. Studying the time evolution of a system, i.e. resolving the associated equations of motion, requires a physical model encoding the interactions between particles. Ideally, at this level of description, this model should be grounded on quantum mechanics. However, solving numerically the electronic structure problem, with so-called *ab initio* methods [4], remains computationally expensive, which limits their application to relatively small systems and on short time scales. A more coarse grained approach, realizing a good compromise between computational efficiency and modeling at the atomic scale, consists in using an empirical potential [5, 6, 7, 8, 9, 10] with a given functional form, involving *a priori* unknown parameters that must be optimized to replicate a set of targeted thermodynamic or structural properties.

In recent years, a third approach has emerged, namely Neural Network potentials (NNPs) [11, 12, 13, 14, 15, 16, 17, 18, 19, 20, 21, 22, 23, 24, 25, 26], which can be seen as the application of machine-learning architectures to the empirical potential approach, learning an energy model from large *ab initio* computation databases. Nowadays, several libraries such as SchnetPack [27], DeepMD-kit [28], MLAtom [29] or FeNNol [30] enable the implementation of NNPs, and large foundation models such as MACE [31, 32] and FeNNix-Bio1 [33] allow general-purpose simulations, covering complete areas of applications of molecular dynamics [31, 32, 33, 24, 34]. Several important advantages over traditional approaches can be highlighted. First, the large number of parameters, whose optimization is fully automated, make NNPs highly flexible and largely transferable across systems. Second, they

inherently handle chemical reactions, which most classical empirical force fields don't. Finally, again thanks to the large number of parameters, NNPs can achieve close-to quantum-mechanical accuracy, only for a fraction of the computation cost of *ab initio* methods. However, they remain significantly more expensive to evaluate than traditional empirical potentials, which motivates the development of algorithms increasing the speed of simulation based on NNPs without loosing their high accuracy.

In a molecular dynamics simulation, the number of evaluations of the gradient of the potential energy per unit of physical time is proportional to the time discretization step size  $\delta$ . The maximum value of this parameter which preserves stability and accuracy of the simulation is limited by the highest-frequency motions of the system, such as chemical bond vibrations. A well-known approach to increase the step size used in classical integrators such as BAOAB [35, 36] is called multi time-stepping [37, 38, 39] (MTS). When applied to an empirical force field model, it consists in treating the fast-varying short-range forces within a small step size  $\delta$ , while only applying the long-range, more regular forces at larger time step  $\Delta = n\delta$ . This effectively increases the speed of simulation by reducing the rate at which expensive long-range forces are computed. Note that although MTS simulations are stable and accurate for  $\Delta$  several times larger than  $\delta$ , its maximum value is also bounded, this time by resonance phenomena [40, 41] resulting from a coupling of internal frequencies of the molecular system with nonphysical periodicity created by the various time steps, which can induce numerical instabilities for large values of  $\Delta$ . Despite these limitations (for which various alternative methods have also been proposed [42, 43, 44, 45, 46]), MTS methods such as RESPA [37] or BAOAB-RESPA1 [39] are widely implemented and used.

MTS schemes have also been shown to be applicable to Ab Initio MD (AIMD) [47], and several recent works studied their use in machine learning approaches [48, 49, 50, 51, 52]. Note that the principle of MTS as described above is not readily applicable to NNPs, since there is no natural decomposition of the forces into "cheap" and "expensive" parts. Recently, we proposed [52] a so-called distilled multi-time-step (DMTS) strategy for NNPs based on distillation [53, 54] of the FeNNix-Bio1(M) foundation model [33] which was performed via the FeNNol [30] library. In this strategy, a small, less precise but fast-to-evaluate model is trained on data labeled with the FeNNix-Bio1(M) model instead of Density Functional Theory. Then, following the MTS procedure, this small model is applied in several iterations of an inner loop, before being corrected by an application of the difference between the large and small force models in an external loop. Therefore, by reducing the number of computations of the large expensive model, simulation speed is increased, enabling longer stable simulations.

As proposed in several previous works [55, 21, 56, 57, 58, 59], another path to accelerating simulation speed with ML models is to use non-conservative forces (i.e. forces that are not constrained to deriving from a potential energy). Indeed, directly predicting the interatomic forces enables to bypass the costly backpropagation step required to compute conservative forces, thus improving computational efficiency at fixed model architecture. However, Bigi et al. [60] identified severe simulation artifacts induced by this approach and alternatively propose to use non-conservative forces in a MTS scheme. In their approach, a single model is trained to output both conservative and non-conservative forces: non-conservative forces are used at every step of the simulation while conservative ones are only evaluated every few steps. In the present article, we follow a similar direction and extend our DMTS procedure to the use of non-conservative forces, which we denote DMTS-NC, in order to further accelerate simulations without loss in accuracy. Now, the large NNP model is distilled into a small force model without the constraint of deriving from an energy. This distillation step enables to greatly reduce the cost of the model used in the internal steps of the MTS scheme, compared to the unified model proposed in [60]. Furthermore, by directly learning forces instead of energies (in particular, their computation don't require differentiation procedures anymore), both training and evaluation of the model are faster than the small models used previously in [52]. In addition, by imposing several physical priors such as equivariance under rotation and cancellation of atomic force components (which are properties that are satisfied by conservative forces), the distilled model is able to closely fit the reference one. We show that the improved agreement between the models, with training reaching a mean absolute error near 1 kcal/mol/Å on a diverse dataset, enables more precise and stable simulations. This in turn allows for a larger external time step, further enhancing the speed and robustness of DMTS schemes with FeNNix-Bio1(M). Importantly, like the original DMTS framework, DMTS-NC is a model-agnostic acceleration strategy, and can be applied in principle to any neural network potential, independently of its specific architecture.

The rest of the article is organized as follows. In Section 2, we describe the architecture and training of the non-conservative model, the associated DMTS-NC integrator, as well as two techniques used to further stabilize the dynamics, namely Hydrogen Mass Repartitioning (HMR) and a revert procedure preventing occasional disagreements between the models. Section 3 is devoted to numerical experiments and validation of the improved stability and speed of DMTC-NC on various molecular systems.

## 2 Methods

**Model architecture.** The architecture of the non-conservative model is a modification of FeNNix-Bio1 [33] in which the neural network learns to directly predict forces instead of energies. By removing the requirement of having conservative forces, i.e. deriving from a potential, certain properties such as Newton’s third law are not guaranteed anymore. However, our architecture is designed to still enforce some physical priors, such as equivariance under rotation and cancellation of atomic force components.

Let us first quickly recall the general architecture of FeNNix-Bio1. In a first step, each atom is embedded in a  $N_f$ -dimensional vector space, describing electronic structure and charge information. This initial geometry-independent embedding is then updated to include local geometric information via two message-passing layers of an equivariant transformer. The first layer considers a high-resolution description of very short range (within a  $R_c^{(sr)} = 3.5 \text{ \AA}$  cutoff) geometry, while the second layer incorporates both short-range and medium-range messages up to a cutoff  $R_c^{(lr)} = 7.5 \text{ \AA}$ . Then, atomic energies for each atom are obtained from mixture-of-experts multi-layer perceptrons, taking the final embeddings as an input, with routing depending on the chemical group of each atom. Finally an explicit screened nuclear repulsion term is added. We refer to [33] for more details.

Let us now describe the non-conservative model. First, the embedding architecture is similar, except that only short-range messages are considered in both layers, letting the model mainly focus on local structure. Since the goal is to use this model in internal loops of a MTS integrator, its main focus is designed to be on short-range forces and the associated high frequencies. At the end of the embedding layers, the description of each atom  $i$  involves a scalar embedding  $x_i \in \mathbb{R}^{N_f}$ , as well as a tensorial embedding  $\hat{V}_i \in \mathbb{R}^{n_l \times (\lambda_{\max}+1)^2}$  that is a collection, along  $n_l$  channels, of geometric tensors of orders up to  $\lambda_{\max}$ . Let us now consider  $n_s$  scalar attention heads and  $n_l$  tensor heads, one for each first-order geometric tensor channel. For each atom  $i$  and each attention head  $h \in \{1, \dots, n_s + n_l\}$ , we form vectors  $q_{ih}$  and  $k_{ih}$  via a linear projection of the scalar embedding  $x_i$  on a subspace of dimension  $n_c$ :

$$\begin{aligned} q_{ih} &= W_{qh} x_i \\ k_{ih} &= W_{kh} x_i, \end{aligned}$$

where, for each head  $h$ ,  $W_{qh}$  and  $W_{kh}$  are weight matrices, optimized during the training.

Denote  $\mathcal{N}(i)$  the neighbor list of atom  $i$ , i.e. the set of all atoms  $j \neq i$  such that the distance  $r_{ij}$  between them is less than or equal to  $R_c^{(sr)}$ . For each  $h \in \{1, \dots, n_s + n_l\}$  and each  $j \in \mathcal{N}(i)$ , denote  $c_{ijh}$  the scaled dot product

$$c_{ijh} = \frac{1}{\sqrt{n_c}} \sum_{k=1}^{n_c} q_{ihk} k_{jkh}.$$

We then denote  $\vec{R}_{ij}$  the vector pointing from  $i$  towards  $j$  and  $(B_h(r_{ij}))_{h \in \{1, \dots, n_s\}}$  a radial basis vector corresponding to the decomposition of  $r_{ij}$  in a basis of  $n_s$  Bessel functions, as described in [61]. Consider now the three-dimensional vector  $F_{ij}$ , such that

$$F_{ij} = \left( \sum_{h=1}^{n_s} c_{ijh} B_h(r_{ij}) \right) \left( \frac{\vec{R}_{ij}}{r_{ij}} + \sum_{h=1}^{n_l} c_{ij(n_s+h)} \vec{V}_{ih} \right) f_c(r_{ij}),$$

where  $\vec{V}_{ih}$  is the vector part of the tensor embedding  $\hat{V}_{ih}$  (i.e. the irreps of order  $\lambda = 1$ ),  $f_c(r_{ij})$  is a polynomial cutoff function going smoothly to zero at the short-range cutoff distance  $R_c^{(sr)}$ , as defined in [61]. The final force vector acting on atom  $i$  is then given by

$$F_i = \sum_{j \in \mathcal{N}(i)} (F_{ij} - F_{ji}) + F_{rep,i} \in \mathbb{R}^3,$$

where and  $F_{rep} = -\nabla E_{rep}$  is the same short-range screened nuclear repulsion term as in FeNNix-Bio1, whose expression is analytic and defined using the element-pair-specific NLH parametrization of [62]:

$$E_{rep}(r_{ij}) = \frac{Z_i Z_j}{4\pi \varepsilon_0 r_{ij}} \sum_{n=1}^3 a_{nij} e^{-b_{nij} r_{ij}},$$

with  $Z_i$  the atomic number of atom  $i$ ,  $r_{ij}$  the distance between atoms  $i$  and  $j$ , and  $a_{nij}, b_{nij}$  parameters that depend on the unordered pair of species  $Z_i, Z_j$  that were obtained via a fit to *ab initio* references in [62].

Note that  $F_i$  explicitly depends on the tensorial embedding  $\hat{V}_i$ , while in the original architecture of FeNNix-Bio1 it is only used as an internal descriptor in the embedding phase, and not given as an input to the perceptrons that output the final energies. In particular, here the functional form of  $F_i$  ensures that the sum of the forces over all atoms is zero (and more generally the sum of the  $F_i$  over any connected component of the interaction graph of the atoms is also zero). In addition, all the  $F_{ij}$ , and therefore the  $F_i$  too, are equivariant under rotation.

We conclude this paragraph with the parameter values. In FeNNix-Bio1(M),  $N_f = 176$ ,  $n_c = 16$ ,  $\lambda_{max} = 3$ ,  $n_l = 4$  and  $n_s = 10$ . In the small NC model, we have  $N_f = 64$ ,  $n_c = 8$ ,  $\lambda_{max} = 1$ ,  $n_l = 2$  and  $n_s = 8$ . For the sake of completeness, let us mention that in the initial geometry-independent embedding, the number of charge equilibration channels is  $N_Q = 32$  in FeNNix-Bio1(M), and  $N_Q = 8$  in the NC model, the species embedding neural network involves one layer of 256 neurons in FeNNix-Bio1(M) and only 64 in the NC model. In the message-passing phase, the attention mechanism involves  $h_s = 16$  scalar attention heads in FeNNix-Bio1(M) and  $h_s = 4$  in the NC model, and a two hidden-layers neural network, with respectively 352 and 176 neurons in FeNNix-Bio1(M) and a one-hidden-layer neural network with 64 neurons in the NC model. Finally, the polynomial  $f_c(r_{ij})$  is of order 8 in FeNNix-Bio(M), and 5 in the NC model. This results in a total number of 286 736 parameters in the NC model, compared to 9 526 855 for FeNNix-Bio1(M).

**Model training.** Following the principle of knowledge distillation [53, 54], as applied in [52], the non-conservative force model is trained as a distilled version of the larger FeNNix-Bio1(M) [33] NNP. A subset of conformations of the SPICE2 dataset [63, 64] is evaluated with FeNNix-Bio1(M), which then constitutes the training dataset for the non-conservative force model. This dataset contain a variety of small organic molecules and biologically relevant complexes, thus covering a wide chemical space.

The training was done for 2200 epochs with 1000 batches of 128 conformations per epoch. We used the Muon optimizer [65], with an initial learning rate of  $1.0 \times 10^{-5}$ , linearly increasing up to  $5.0 \times 10^{-4}$  after a warm-up phase, then decreasing down to a final rate of  $1.0 \times 10^{-6}$  according to a cosine one-cycle learning-rate schedule. The total training, performed on a Nvidia A100 40GB GPU, took 28 hours and 47 minutes. The resulting model, which directly aims at fitting the force vectors produced by FeNNix-Bio1(M) instead of the energies, ends up achieving excellent agreement with the data, reaching a final mean absolute error of MAE=1.46kcal/mol and a root mean square error of RMSE=2.33kcal/mol, a significantly lower value than for the small conservative model of [52], for which MAE=3.44kcal/mol and RMSE=5.53kcal/mol.

**MTS integrator.** Let us denote  $U : \mathbb{R}^d \rightarrow \mathbb{R}$  a potential energy function, and  $\mathcal{L}$  the infinitesimal generator of associated Langevin dynamics. Most single time step methods rely on so-called splitting of the dynamics. For instance, the BAOAB method [35, 36] consists in splitting the Langevin process into three parts A, B and O, corresponding respectively to free transport, acceleration and fluctuation/dissipation, which comes down to splitting the generator as  $\mathcal{L} = \mathcal{L}_A + \mathcal{L}_B + \mathcal{L}_O$  and simulating successively the parts B-A-O-A-B, thanks to the Trotter/Strang formula

$$e^{t\mathcal{L}} = e^{\frac{t}{2}\mathcal{L}_B} e^{\frac{t}{2}\mathcal{L}_A} e^{t\mathcal{L}_O} e^{\frac{t}{2}\mathcal{L}_A} e^{\frac{t}{2}\mathcal{L}_B} + \mathcal{O}_{t \rightarrow 0}(t^3).$$

Multi-Time-Step (MTS) methods such as BAOAB-RESPA push the splitting of the dynamics one step further, by decomposing the force vector field  $-\nabla U = F_S + F_L$  and considering separately the associated accelerations  $\mathcal{L}_{B_S}$  and  $\mathcal{L}_{B_L}$ . In a classical force field,  $F_S$  typically gathers the fast-varying, easy to compute short-range forces and  $F_L$  includes more regular many-body or long-range forces that are more expensive to evaluate.

Given a time step  $\delta > 0$ , denote  $Q_\delta$  one transition of the BAOAB chain associated with the force  $F_S$ , namely

$$Q_\delta = e^{\frac{\delta}{2}\mathcal{L}_{B_S}} e^{\frac{\delta}{2}\mathcal{L}_A} e^{\delta\mathcal{L}_O} e^{\frac{\delta}{2}\mathcal{L}_A} e^{\frac{\delta}{2}\mathcal{L}_{B_S}}.$$

Then, by denoting  $\Delta = n\delta$  some multiple of  $\delta$ , the BAOAB-RESPA MTS scheme relies on the following approximation of the continuous dynamics:

$$e^{\Delta\mathcal{L}} \approx e^{\frac{\Delta}{2}\mathcal{L}_{B_L}} (Q_\delta)^n e^{\frac{\Delta}{2}\mathcal{L}_{B_L}}.$$

In other words, by denoting  $x$  and  $v$  position and velocity vectors, one transition of the integrator consists in the succession of the following steps:

1.  $v \leftarrow v - \frac{\Delta}{2} M^{-1} F_L(x)$ .
2. Perform  $n$  times the BAOAB scheme associated with  $F_S$  with time step  $\delta$ .

$$3. \quad v \leftarrow v - \frac{\Delta}{2} M^{-1} F_L(x).$$

Note that in this method,  $F_S$  and  $F_L$  are not required to be conservative forces, i.e. gradients of an energy function. They only need to satisfy  $F_S + F_L = -\nabla U$ . In DMTS-NC,  $F_S$  is the smaller, faster to evaluate machine-learned model approximating  $\nabla U$  that we described above and  $F_L = -\nabla U - F_S$ . The term distillation refers to the fact that the data on which the smaller model  $F_S$  is trained is labeled using the larger model  $\nabla U$ . To sum up, the full procedure is given in Algorithm 1.

---

**Algorithm 1** MTS Integration Step with FENNIX Force Splitting

---

**Input:** FENNIX<sub>large</sub>( $x$ ) the reference force field evaluated at configuration  $x$ , FENNIX<sub>NC</sub>( $x$ ) the cheaper non-conservative force model,  $M$  the mass matrix,  $\Delta$  the external time-step,  $n$  the number of iterations of the internal loop.

---

```

1: if first_step then
2:    $F_{NC} \leftarrow FENNIX_{NC}(x)$ 
3:    $F \leftarrow FENNIX_{large}(x)$ 
4: end if
5:  $v \leftarrow v + \frac{\Delta}{2} M^{-1}(F - F_{NC})$ 
6: for  $i = 1$  to  $n$  do
7:    $v \leftarrow v + \frac{\Delta}{2n} M^{-1} F_{NC}$ 
8:    $x \leftarrow x + \frac{\Delta}{2n} v$ 
9:    $v \leftarrow \text{thermo} \left( v, \frac{\Delta}{n} \right)$  ▷ Apply thermostat
10:   $x \leftarrow x + \frac{\Delta}{2n} v$ 
11:   $F_{NC} \leftarrow FENNIX_{NC}(x)$ 
12:   $v \leftarrow v + \frac{\Delta}{2n} M^{-1} F_{NC}$ 
13: end for
14:  $F \leftarrow FENNIX_{large}(x)$ 
15:  $v \leftarrow v + \frac{\Delta}{2} M^{-1}(F - F_{NC})$ 

```

---

**Hydrogen Mass Repartitioning.** The well-known phenomenon of resonances [40, 41] that limits the maximum usable value of  $\Delta$  can be mitigated in various ways. A standard procedure, applied for instance in [39], and which doesn't impair significantly sampling properties is called Hydrogen Mass Repartitioning (HMR) [66]. It consists in increasing the mass of hydrogen atoms (in our simulations, by 3.0 Daltons) and redistributing the deficit over heavier atoms in order to preserve the total mass of each molecule. This has the effect of red-shifting the frequency of intramolecular bond and angle motions, allowing in turn to increase the external time step  $\Delta$ , without biasing configurational sampling (that only depends on potential energy, which is unchanged), nor the temperature (whose distribution doesn't depend on the mass). In addition, as shown below in Section 3 and already noted in [39, 52], by preserving the mass of each molecule, dynamic properties such as diffusion coefficients are not significantly impacted either, contrary to other methods [43, 44, 45].

**Preventing rare disagreements.** In addition to the issue of resonances, intrinsic to multi-time-stepping, a specific pitfall to consider in DMTS is the possibility that on rare occasions,  $F_S$  and  $-\nabla U$  disagree a lot, which can make the dynamics crash rapidly because of the abnormally strong applied force  $F_L = -\nabla U - F_S$ . This type of situation, which can for instance occur when the system explores regions of the configurational space for which less data exists in the training set, resulting in holes in the force surface of the small model, is difficult to anticipate (contrary to the problem of resonances, that are visible very early in the simulation). Indeed, such a rare event can happen after a long simulation, without any issues until then.

One way of resolving this caveat, proposed in [52], relies on an active learning procedure. It consists in fine-tuning the small model based on data frames, collected automatically during an initial simulation, for which the difference between the small and large models exceed some unrealistic threshold. In addition to being system-specific, collecting the problematic data can take a long time if those "holes" rarely appear (and potentially very

long simulations can be required post fine-tuning to validate that the new model is fully stable). Instead, a simple test can be done on the fly: at each time step, if the difference between the two force models (or some indirect indicator such as temperature) exceeds the threshold, rewind the dynamics by one time step and replace DMTS by STS for a given amount of steps, then go back to multi-time-stepping. We refer to these temporary switches as "reverts". Since those events are rare, the whole procedure can be implemented in order to not impact the overall simulation speed.

However, overall, as we will show in Section 3, the non-conservative model fits better the forces produced by FeNNix-Bio1(M) than the small conservative model of [52], and fewer, if any, holes are encountered, therefore making the generic model robust without relying on system-specific fine-tuning. In addition, since the NC model is less likely to deviate from the larger model after a few small time steps, DMTS-NC is robust for larger values of  $\Delta$ . As we will show, the maximum usable time step in this new model corresponds to the classical "step size region" where resonances between the forces applied in the various time steps start to appear.

### 3 Numerical results

The goal of this section is to validate speed, stability and sampling accuracy of the DMTS-NC method, on bulk water boxes of various sizes and two solvated protein systems. All simulations were performed in periodic boundary conditions, applying the Langevin thermostat with a fluctuation/dissipation profile given by a  $1\text{ ps}^{-1}$  friction parameter and a 300 K temperature. For DMTS and DMTS-NC, HMR is systematically activated. Training and MD used the FeNNol [30] Python library coupled to the Tinker-HP package [67, 68] within its Deep-HP module [48] on a single NVIDIA A100 40GB GPU card.

#### 3.1 Bulk water

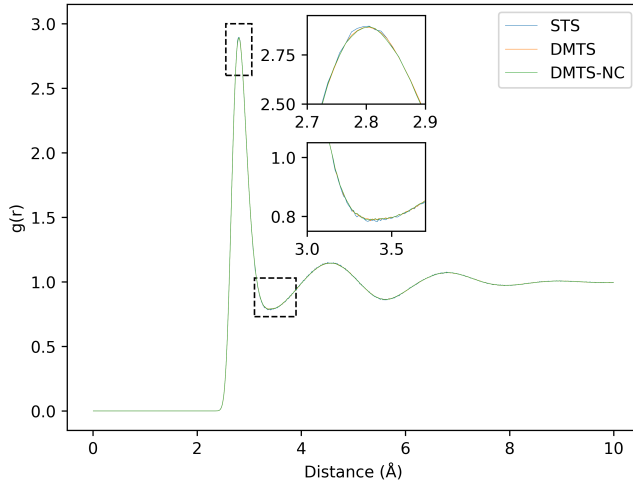
In the following, we compare, for various sizes of bulk water boxes and various time steps, the STS BAOAB integrator, DMTS with the small conservative model used in [52] and DMTS-NC, the multi-time-step method BAOAB-RESPA with the non-conservative force model. Figure 1 shows oxygen-oxygen radial distributions (computed with FeNNol), as well as distributions of temperatures and potential energies across simulations. In particular, empirical distributions of temperature (known to be sensitive to numerical instabilities due to multi-time-stepping) are plotted along the equilibrium theoretical distribution, given by  $\frac{T}{d}\chi^2(d)$ , where  $T$  is the equilibrium average temperature (here, 300 K),  $d$  is the total configurational dimension of the system (i.e. three times the number of atoms) and  $\chi^2(d)$  is the Chi-squared distribution with  $d$  degrees of freedom. In addition, Table 3 sums up the average potential energies and temperatures.

Table 1 shows the speed of the algorithms expressed in nanoseconds of simulation per day, highlighting the significant acceleration of DMTS-NC with respect to conservative-model DMTS and to STS. Note that in addition to being faster, thanks to a better fit to the training data, DMTS-NC exhibits fewer numerical instabilities, and the maximum usable time step is limited by classical MTS resonances instead of the problem of abnormal model disagreements as described in Section 2. Results show that DMTS-NC provides an acceleration ranging from 294% to 431% with respect to STS, and from 30.8% to 55.7% with respect to conservative DMTS.

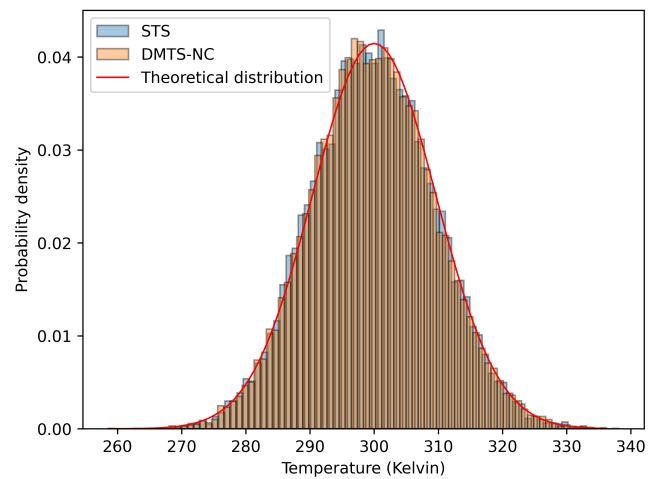
When analyzing MTS strategies (and more generally any method aiming at accelerating simulation speed), a standard sanity check consists in computing the diffusion coefficient, a dynamic property that measures the tendency of particles to drift in the system. A too negative impact of this quantity can indicate a limitation in the effective sampling rate, which therefore reduces the computational gain since a longer trajectory would then be necessary to keep the same amount of sampling. As explained in [39], a good rule of thumb is to check whether the acceleration rate is higher than the loss rate in the diffusion constant. Here, we computed these constants with the Einstein formula, using the Tinker 8 [69] implementation, from 2ns of simulation of the 4800 atom water box, with frames saved every 0.1ps. The results are the following. The average diffusion constant associated with FeNNix-Bio1(M) STS is 1.73 and 1.59 if HMR is activated. With DMTS, we find 1.43 (i.e. 17.3% loss with respect to STS, and 10.1% loss with respect to STS with HMR), and with DMTS-NC, we find 1.41 (i.e. 18.7% loss with respect to STS, and 11.3% loss with respect to STS with HMR). In particular, we see that these percentages are much smaller than the rates of acceleration in simulation speed.

#### 3.2 Solvated proteins

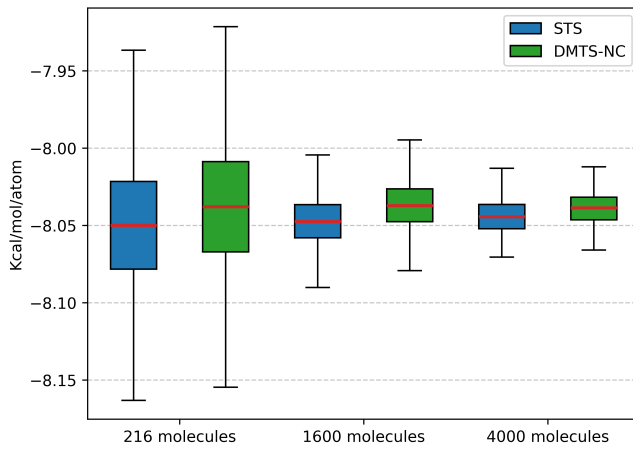
We next turn to solvated protein systems. In this section, we compare speed of simulation, shown in Table 2, average potential energy and average temperature of solvated phenol-lysosyme protein-ligand complex (16221



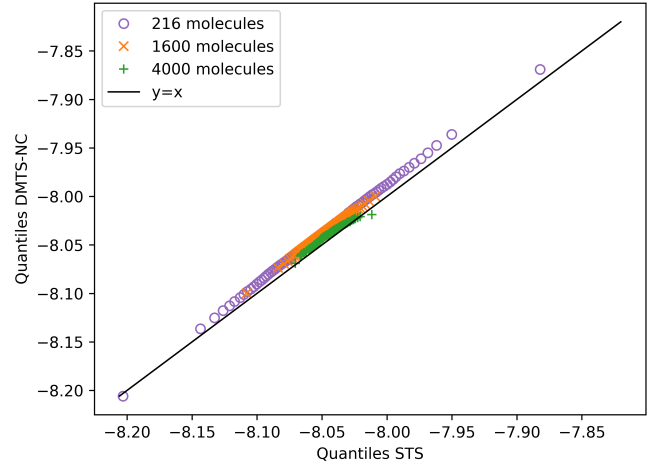
(a) Oxygen-oxygen radial distribution (1600 water molecules)



(b) Temperature distribution (216 water molecules)



(c) Potential energy distributions: box plots



(d) Potential energy distributions: Q-Q plots

Figure 1: Sampling properties of bulk water simulations. All data was collected from 2 nanosecond simulations, with one frame saved per picosecond. As the graphs above show, radial distributions are not affected by the use of DMTS-NC compared to DMTS or STS, temperatures fit the equilibrium theoretical distribution, and samples of potential energies, especially represented on the quantile-quantile plot, highlight the low-bias constant-variance deviation of the distributions from STS to DMTS-NC, as expected for a multi-time-step method in a stable regime.

	Number of atoms			Numerical instabilities
	648	4800	12000	
STS	36.89	9.08	3.63	No
DMTS 1-5fs	69.54	30.17	11.95	No
DMTS 1-6fs	80.62	34.34	NaN (13.10 before crash)	Data holes (random crashes)
DMTS 1-7fs	NaN			
DMTS-NC 1-5fs	91.13	32.69	12.39	No
DMTS-NC 1-6fs	103.67	36.15	13.67	No
DMTS-NC 1.625-6.5fs	108.29	41.10	15.64	No
DMTS-NC 1-7fs	114.11	39.72	13.56	High temperature (resonances)
Maximum acceleration DMTS-NC/DMTS	55.7%	36.2%	30.8%	
Maximum acceleration DMTS-NC/STS	294%	453%	431%	

Table 1: Simulation performances for bulk water systems, expressed in nanoseconds per day.

atoms) and solvated dihydrofolate reductase protein (DHFR, 23558 atoms). Results show that DMTS-NC provides an acceleration with respect to STS of 340% for phenol-lysosyme and 309% for DHFR, an acceleration with respect to the generic conservative DMTS of 31.6% for phenol-lysosyme and 28.3% for DHFR, and finally, an acceleration with respect to the fine-tuned (after active learning) conservative DMTS of 16.4% for phenol-lysosyme and 15.1% for DHFR. Note that in all simulations, DMTS-NC uses a generic, non-fine-tuned model.

After 5ns of simulation of phenol-lysosyme we get an average temperature of  $300.15 \pm 1.99$ K (the number after the plus-minus sign corresponding to the empirical standard deviation) with STS and  $301.51 \pm 1.99$ K with DMTS-NC with 1.25 – 5fs time steps. For potential energy, we find  $-7.87 \pm 0.009$ kcal/mol/atom with STS and  $-7.85 \pm 0.009$ kcal/mol/atom with DMTS-NC. Regarding DHFR with the same simulation parameters, the average temperature with STS is  $299.97 \pm 1.64$ K and  $302.26 \pm 1.64$ K with DMTS-NC. For average potential energy we find  $-7.82 \pm 0.008$ kcal/mol/atom with STS and  $-7.79 \pm 0.007$ kcal/mol/atom with DMTS-NC. Results are gathered in Table 3. Similarly to simulations of bulk water, note the low-bias constant-variance deviation of the distributions from STS to DMTS-NC, as expected for a multi-time-step method in a stable regime. Overall, results show that an external time-step of  $\Delta = 5$ fs yields stable and accurate simulations, while resonance problems start to arise for larger values of  $\Delta$ . Finally, in Figure 2, we show the time evolution of the protein backbone RMSD and the ligand’s Distance to Bound Configuration (DBC) during a 20ns simulation of the solvated lysosyme-phenol.

Integrator	Phenol-lysosyme	DHFR	Numerical instabilities
	Speed	Speed	
STS	2.55	1.85	No
DMTS 1.75-3.5	6.59	4.46	No
DMTS 1-4	NaN		
Fine-tuned DMTS 2-4	7.45	4.97	Not anymore
DMTS-NC 1-4	7.20	4.886	No
DMTS-NC 1-5	8.42	5.57	No
DMTS-NC 1.25-5	8.67	5.72	No
DMTS-NC 1.1-5.5	NaN		
DMTS-NC 1-6	9.16	5.97	Data holes
Maximum acceleration DMTS-NC/DMTS	31.6% w.r.t generic, 16.4% w.r.t. fine-tuned	28.3% w.r.t generic, 15.1% w.r.t. fine-tuned	
Maximum acceleration DMTS-NC/STS	340%	309%	

Table 2: Simulation performances for the two ligand-protein systems, expressed in nanoseconds per day.

System		Integrator	Temperature (K)	Potential energy (kcal/mol/atom)
Water boxes	216 molecules	STS	299.84 $\pm$ 9.57	-8.05 $\pm$ 0.042
		DMTS-NC	299.87 $\pm$ 9.56	-8.04 $\pm$ 0.043
	1600 molecules	STS	300.09 $\pm$ 3.60	-8.05 $\pm$ 0.017
		DMTS-NC	299.93 $\pm$ 3.54	-8.04 $\pm$ 0.016
	4000 molecules	STS	300.61 $\pm$ 2.93	-8.04 $\pm$ 0.014
		DMTS-NC	299.69 $\pm$ 2.22	-8.04 $\pm$ 0.011
Solvated proteins	phenol-lysosyme	STS	300.15 $\pm$ 1.99	-7.87 $\pm$ 0.009
		DMTS-NC	301.51 $\pm$ 1.99	-7.85 $\pm$ 0.009
	DHFR	STS	299.97 $\pm$ 1.64	-7.82 $\pm$ 0.008
		DMTS-NC	302.26 $\pm$ 1.64	-7.79 $\pm$ 0.007

Table 3: Average temperatures and potential energies. The numbers after the plus-minus signs correspond to the empirical standard deviations.

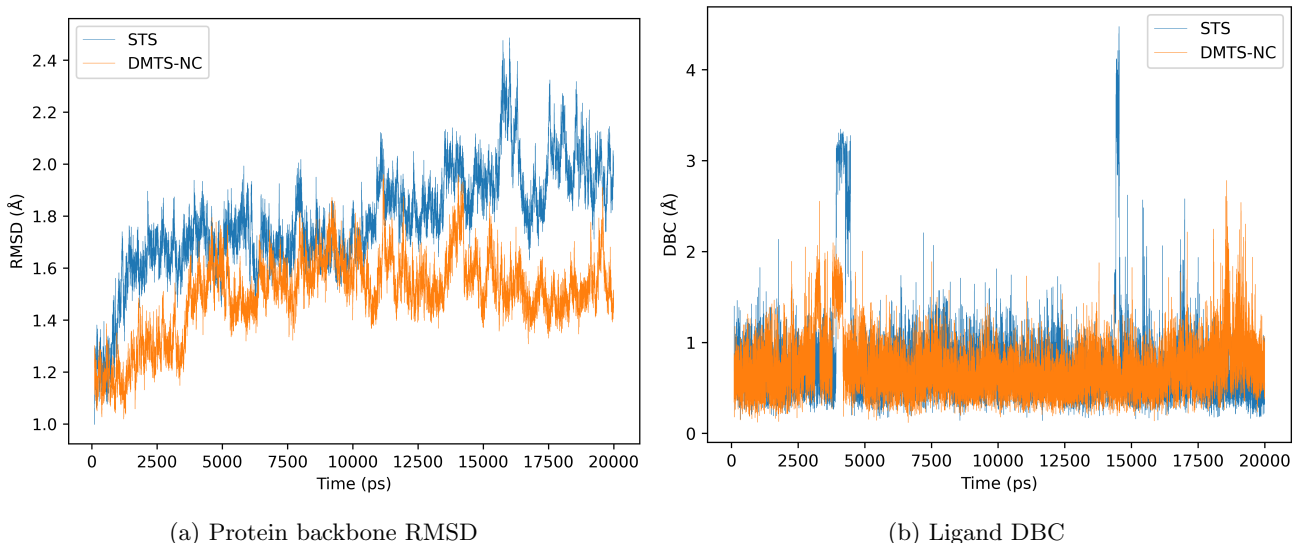


Figure 2: Time evolution of the protein backbone RMSD and the ligand’s Distance to Bound Configuration (DBC) during a 20ns simulation of the solvated lysosyme-phenol. The DMTS-NC integrator uses 1.25 – 5fs time steps.

## Conclusion

We have shown that by combining model distillation, non-conservative force models with imposed physical priors and multi-time-step strategies, we are able to significantly accelerate molecular dynamics simulations with neural network potentials, while preserving near-*ab initio* accuracy. DMTS-NC can be applied to any neural network potential, independently of its specific architecture. The presented speedups will contribute to further reduce the performance gap with force fields. Next works will aim at optimizing the present implementation to improve performances towards extending tests to more complex systems and more subtle sampling properties. We will also leverage other types of acceleration methods such as further splits approaches inspired by RESPA-1 and RESPA-2 techniques [70, 39] and Velocity Jumps [46].

## Competing interests

Louis Lagardère and Jean-Philip Piquemal are shareholders and co-founders of Qubit Pharmaceuticals. All the remaining authors declare no conflict of interest.

## Acknowledgement

This work has received funding from the European Research Council (ERC) under the European Union’s Horizon 2020 research and innovation program (grant agreement No 810367), project EMC2 (JPP). Computations have been performed at IDRIS (Jean Zay) on GENCI Grants: no A0150712052 (J.-P. P.).

## Code availability

Calculations were performed using the FeNNol library: <https://github.com/FeNNol-tools/FeNNol> and the Tinker-HP package: <https://github.com/TinkerTools/tinker-hp>

## Data availability

Pretrained models are available on Github at: <https://github.com/FeNNol-tools/FeNNol-PMC>

## References

- [1] B. Leimkuhler and C. Matthews. *Molecular Dynamics*. Springer, 2015.
- [2] M. P. Allen and D. J. Tildesley. *Computer Simulation of Liquids*. Oxford University Press, 2017.
- [3] G Ciccotti, C Dellago, M Ferrario, E R Hernández, and M E Tuckerman. Molecular simulations: past, present, and future (a topical issue in EPJB). *Eur. Phys. J. B*, 95(1), January 2022.
- [4] F. Jensen. *Introduction to Computational Chemistry*. Wiley, 2017.
- [5] P. Ren and J. W. Ponder. Polarizable Atomic Multipole Water Model for Molecular Mechanics Simulation. *The Journal of Physical Chemistry B*, 107(24):5933–5947, 2003.
- [6] M. M. Reif, P. H. Hünenberger, and C. Oostenbrink. New Interaction Parameters for Charged Amino Acid Side Chains in the GROMOS Force Field. *Journal of Chemical Theory and Computation*, 8(10):3705–3723, 2012.
- [7] J. A. Maier, C. Martinez, K. Kasavajhala, L. Wickstrom, K. E. Hauser, and C. Simmerling. ff14sb: Improving the Accuracy of Protein Side Chain and Backbone Parameters from ff99sb. *Journal of Chemical Theory and Computation*, 11(8):3696–3713, 2015.
- [8] M. J. Robertson, J. Tirado-Rives, and W. L. Jorgensen. Improved Peptide and Protein Torsional Energetics with the OPLS-AA Force Field. *Journal of Chemical Theory and Computation*, 11(7):3499–3509, 2015.

[9] J. Huang, S. Rauscher, G. Nawrocki, T. Ran, M. Feig, B. L. de Groot, H. Grubmueller, and A. D. MacKerell, Jr. CHARMM36m: an improved force field for folded and intrinsically disordered proteins. *NATURE METHODS*, 2017.

[10] Alexander D. MacKerell. *Chapter 7 Empirical Force Fields for Proteins: Current Status and Future Directions*, volume 1 of *Annual Reports in Computational Chemistry*, pages 91–102. Elsevier, 2005.

[11] Jörg Behler and Michele Parrinello. Generalized neural-network representation of high-dimensional potential-energy surfaces. *Physical Review Letters*, 98(14):146401, 2007.

[12] Albert P Bartók, Mike C Payne, Risi Kondor, and Gábor Csányi. Gaussian approximation potentials: The accuracy of quantum mechanics, without the electrons. *Physical Review Letters*, 104(13):136403, 2010.

[13] Khosrow Shakouri, Jörg Behler, Jörg Meyer, and Geert-Jan Kroes. Accurate neural network description of surface phonons in reactive gas–surface dynamics: N<sub>2</sub>+ ru (0001). *The Journal of Physical Chemistry Letters*, 8(10):2131–2136, 2017.

[14] Justin S Smith, Olexandr Isayev, and Adrian E Roitberg. Ani-1: an extensible neural network potential with dft accuracy at force field computational cost. *Chemical Science*, 8(4):3192–3203, 2017.

[15] K. T. Schütt, P.-J. Kindermans, H. E. Sauceda, S. Chmiela, A. Tkatchenko, and K.-R. Müller. Schnet: a continuous-filter convolutional neural network for modeling quantum interactions. In *Proceedings of the 31st International Conference on Neural Information Processing Systems*, NIPS’17, page 992–1002, Red Hook, NY, USA, 2017. Curran Associates Inc.

[16] Stefan Chmiela, Huziel E Sauceda, Klaus-Robert Müller, and Alexandre Tkatchenko. Towards exact molecular dynamics simulations with machine-learned force fields. *Nature Communications*, 9(1):1–10, 2018.

[17] Andrea Grisafi and Michele Ceriotti. Incorporating long-range physics in atomic-scale machine learning. *The Journal of Chemical Physics*, 151(20):204105, 2019.

[18] Roman Zubatyuk, Justin S. Smith, Jerzy Leszczynski, and Olexandr Isayev. Accurate and transferable multitask prediction of chemical properties with an atoms-in-molecules neural network. *Science Advances*, 5(8):eaav6490, 2019.

[19] Christian Devereux, Justin S. Smith, Kate K. Huddleston, Kipton Barros, Roman Zubatyuk, Olexandr Isayev, and Adrian E. Roitberg. Extending the applicability of the ani deep learning molecular potential to sulfur and halogens. *Journal of Chemical Theory and Computation*, 16(7):4192–4202, 2020.

[20] Oliver T Unke, Stefan Chmiela, Michael Gastegger, Kristof T Schütt, Huziel E Sauceda, and Klaus-Robert Müller. Spookynet: Learning force fields with electronic degrees of freedom and nonlocal effects. *Nature Communications*, 12(1):1–14, 2021.

[21] Johannes Gasteiger, Florian Becker, and Stephan Günnemann. Gemnet: Universal directional graph neural networks for molecules. *Advances in Neural Information Processing Systems*, 34:6790–6802, 2021.

[22] Andrea Grisafi, Jigyasa Nigam, and Michele Ceriotti. Multi-scale approach for the prediction of atomic scale properties. *Chemical Science*, 12(6):2078–2090, 2021.

[23] Albert Musaelian, Simon Batzner, Anders Johansson, Lixin Sun, Cameron J Owen, Mordechai Kornbluth, and Boris Kozinsky. Learning local equivariant representations for large-scale atomistic dynamics. *Nature Communications*, 14(1):579, 2023.

[24] Thomas Plé, Louis Lagardère, and Jean-Philip Piquemal. Force-field-enhanced neural network interactions: from local equivariant embedding to atom-in-molecule properties and long-range effects. *Chemical Science*, 14:12554–12569, 2023.

[25] Oliver T. Unke, Martin Stöhr, Stefan Ganscha, Thomas Unterthiner, Hartmut Maennel, Sergii Kashubin, Daniel Ahlin, Michael Gastegger, Leonardo Medrano Sandonas, Joshua T. Berryman, Alexandre Tkatchenko, and Klaus-Robert Müller. Biomolecular dynamics with machine-learned quantum-mechanical force fields trained on diverse chemical fragments. *Science Advances*, 10(14):eadn4397, 2024.

[26] Adil Kabylda, J. Thorben Frank, Sergio Suárez-Dou, Almaz Khabibrakhmanov, Leonardo Medrano Sandonas, Oliver T. Unke, Stefan Chmiela, Klaus-Robert Müller, and Alexandre Tkatchenko. Molecular simulations with a pretrained neural network and universal pairwise force fields. *Journal of the American Chemical Society*, 147(37):33723–33734, 2025.

[27] Kristof T Schütt, Stefaan S P Hessmann, Niklas W A Gebauer, Jonas Lederer, and Michael Gastegger. SchNetPack 2.0: A neural network toolbox for atomistic machine learning. *J. Chem. Phys.*, 158(14):144801, April 2023.

[28] Jinzhe Zeng, Duo Zhang, Denghui Lu, Pinghui Mo, Zeyu Li, Yixiao Chen, Marián Rynik, Li’ang Huang, Ziyao Li, Shaochen Shi, Yingze Wang, Haotian Ye, Ping Tuo, Jabin Yang, Ye Ding, Yifan Li, Davide Tisi, Qiyu Zeng, Han Bao, Yu Xia, Jiameng Huang, Koki Muraoka, Yibo Wang, Junhan Chang, Fengbo Yuan, Sigrbjørn Løland Bore, Chun Cai, Yinnian Lin, Bo Wang, Jiayan Xu, Jia-Xin Zhu, Chenxing Luo, Yuzhi Zhang, Rhys E A Goodall, Wenshuo Liang, Anurag Kumar Singh, Sikai Yao, Jingchao Zhang, Renata Wentzcovitch, Jiequn Han, Jie Liu, Weile Jia, Darrin M York, Weinan E, Roberto Car, Linfeng Zhang, and Han Wang. DeePMD-kit v2: A software package for deep potential models. *J. Chem. Phys.*, 159(5), August 2023.

[29] Pavlo O Dral, Fuchun Ge, Yi-Fan Hou, Peikun Zheng, Yuxinxin Chen, Mario Barbatti, Olexandr Isayev, Cheng Wang, Bao-Xin Xue, Max Pinheiro, Jr, Yuming Su, Yiheng Dai, Yangtao Chen, Lina Zhang, Shuang Zhang, Arif Ullah, Quanhao Zhang, and Yanchi Ou. MLatom 3: A platform for machine learning-enhanced computational chemistry simulations and workflows. *J. Chem. Theory Comput.*, 20(3):1193–1213, February 2024.

[30] Thomas Plé, Olivier Adjoua, Louis Lagardère, and Jean-Philip Piquemal. FeNNol: An efficient and flexible library for building force-field-enhanced neural network potentials. *The Journal of Chemical Physics*, 161(4):042502, 07 2024.

[31] Ilyes Batatia, David P Kovacs, Gregor Simm, Christoph Ortner, and Gábor Csányi. Mace: Higher order equivariant message passing neural networks for fast and accurate force fields. *Advances in Neural Information Processing Systems*, 35:11423–11436, 2022.

[32] Dávid Péter Kovács, J. Harry Moore, Nicholas J. Browning, Ilyes Batatia, Joshua T. Horton, Yixuan Pu, Venkat Kapil, William C. Witt, Ioan-Bogdan Magdău, Daniel J. Cole, and Gábor Csányi. Mace-off: Short-range transferable machine learning force fields for organic molecules. *Journal of the American Chemical Society*, 147(21):17598–17611, 2025.

[33] Thomas Plé, Olivier Adjoua, Anouar Benali, Evgeny Posenitskiy, Corentin Villot, Louis Lagardère, and Jean-Philip Piquemal. A foundation model for accurate atomistic simulations in drug design. *preprint ChemRxiv*, DOI: 10.26434/chemrxiv-2025-f1hgn-v4, 2025.

[34] Anouar Benali, Thomas Plé, Olivier Adjoua, Valay Agarawal, Thomas Appelcourt, Marharyta Blazhynska, Raymond Clay III, Kevin Gasperich, Khalid Hossain, Jeongnim Kim, Christopher Knight, Jaron T. Krogel, Yvon Maday, Maxime Maria, Matthieu Montes, Ye Luo, Evgeny Posenitskiy, Corentin Villot, Venkatram Vishwanath, Louis Lagardère, and Jean-Philip Piquemal. Pushing the accuracy limit of foundation neural network models with quantum monte carlo forces and path integrals. *preprint arXiv: 2504.07948*, DOI: 10.48550/arXiv.2504.07948, 2025.

[35] Benedict Leimkuhler and Charles Matthews. Robust and efficient configurational molecular sampling via langevin dynamics. *The Journal of Chemical Physics*, 138(17):174102, 05 2013.

[36] B Leimkuhler and C Matthews. Rational construction of stochastic numerical methods for molecular sampling. *Appl. Math. Res. Express*, June 2012.

[37] M. Tuckerman, B. J. Berne, and G. J. Martyna. Reversible multiple time scale molecular dynamics. *The Journal of Chemical Physics*, 97(3):1990–2001, 08 1992.

[38] Ruhong Zhou, Edward Harder, Huafeng Xu, and BJ Berne. Efficient multiple time step method for use with ewald and particle mesh ewald for large biomolecular systems. *The Journal of chemical physics*, 115(5):2348–2358, 2001.

- [39] Louis Lagardère, Félix Aviat, and Jean-Philip Piquemal. Pushing the limits of multiple-time-step strategies for polarizable point dipole molecular dynamics. *The Journal of Physical Chemistry Letters*, 10(10):2593–2599, 2019.
- [40] J. J. Biesiadecki and R. D. Skeel. Dangers of Multiple Time Step Methods. *Journal of Computational Physics*, 109(2):318 – 328, 1993.
- [41] Q. Ma, J. Izaguirre, and R. Skeel. Verlet-i/r-respa/impulse is Limited by Nonlinear Instabilities. *SIAM Journal on Scientific Computing*, 24(6):1951–1973, 2003.
- [42] Joseph A. Morrone, Thomas E. Markland, Michele Ceriotti, and B. J. Berne. Efficient multiple time scale molecular dynamics: Using colored noise thermostats to stabilize resonances. *The Journal of Chemical Physics*, 134(1):014103, 2011.
- [43] A. Albaugh, M. E. Tuckerman, and T. Head-Gordon. Combining Iteration-Free Polarization with Large Time Step Stochastic-Isokinetic Integration. *Journal of Chemical Theory and Computation*, 15(4):2195–2205, 2019.
- [44] B. Leimkuhler, D. T. Margul, and M. E. Tuckerman. Stochastic, resonance-free multiple time-step algorithm for molecular dynamics with very large time steps. *Molecular Physics*, 111(22-23):3579–3594, 2013.
- [45] D. T. Margul and M. E. Tuckerman. A Stochastic, Resonance-Free Multiple Time-Step Algorithm for Polarizable Models That Permits Very Large Time Steps. *Journal of Chemical Theory and Computation*, 12(5):2170–2180, 2016.
- [46] Nicolaï Gouraud, Louis Lagardère, Olivier Adjoua, Thomas Plé, Pierre Monmarché, and Jean-Philip Piquemal. Velocity jumps for molecular dynamics. *Journal of Chemical Theory and Computation*, 21(6):2854–2866, 2025.
- [47] Elisa Liberatore, Rocco Meli, and Ursula Rothlisberger. A versatile multiple time step scheme for efficient ab initio molecular dynamics simulations. *Journal of Chemical Theory and Computation*, 14(6):2834–2842, 2018. PMID: 29624388.
- [48] Théo Jaffrelot Inizan, Thomas Plé, Olivier Adjoua, Pengyu Ren, Hatice Gokcan, Olexandr Isayev, Louis Lagardère, and Jean-Philip Piquemal. Scalable hybrid deep neural networks/polarizable potentials biomolecular simulations including long-range effects. *Chemical Science*, 14:5438–5452, 2023.
- [49] Xiang Fu, Albert Musaelian, Anders Johansson, Tommi Jaakkola, and Boris Kozinsky. Learning interatomic potentials at multiple scales. In *NeurIPS 2023 AI for Science Workshop*, 2023.
- [50] Reilly Osadchey, Kwangho Nam, and Qiang Cui. Toward improving multiple time step qm/mm simulations with  $\delta$ -machine learning. *The Journal of Physical Chemistry B*, 129(40):10451–10466, 2025. PMID: 40997780.
- [51] François Mouvet, Nicholas J. Browning, Pablo Baudin, Elisa Liberatore, and Ursula Rothlisberger. Machine learning-enhanced multiple time-step ab initio molecular dynamics. *The Journal of Chemical Physics*, 163(18):184115, 11 2025.
- [52] Côme Cattin, Thomas Plé, Olivier Adjoua, Nicolaï Gouraud, Louis Lagardère, and Jean-Philip Piquemal. Accelerating molecular dynamics simulations with foundation neural network models using multiple time steps and distillation. *The Journal of Physical Chemistry Letters*, 17(5):1288–1295, 2026. PMID: 41562233.
- [53] Geoffrey Hinton, Oriol Vinyals, and Jeff Dean. Distilling the knowledge in a neural network. *arXiv preprint arXiv:1503.02531*, 2015.
- [54] Jianping Gou, Baosheng Yu, Stephen J Maybank, and Dacheng Tao. Knowledge distillation: A survey. *International journal of computer vision*, 129(6):1789–1819, 2021.
- [55] Weihua Hu, Muhammed Shuaibi, Abhishek Das, Siddharth Goyal, Anuroop Sriram, Jure Leskovec, Devi Parikh, and C Lawrence Zitnick. Forcenet: A graph neural network for large-scale quantum calculations. *arXiv preprint arXiv:2103.01436*, 2021.
- [56] Yi-Lun Liao, Brandon Wood, Abhishek Das, and Tess Smidt. Equiformer2: Improved equivariant transformer for scaling to higher-degree representations. *arXiv preprint arXiv:2306.12059*, 2023.

[57] Mark Neumann, James Gin, Benjamin Rhodes, Steven Bennett, Zhiyi Li, Hitarth Choubisa, Arthur Hussey, and Jonathan Godwin. Orb: A fast, scalable neural network potential. *arXiv preprint arXiv:2410.22570*, 2024.

[58] Benjamin Rhodes, Sander Vandenhaute, Vaidotas Šimkus, James Gin, Jonathan Godwin, Tim Duignan, and Mark Neumann. Orb-v3: atomistic simulation at scale. *arXiv preprint arXiv:2504.06231*, 2025.

[59] Max Eissler, Tim Korjakow, Stefan Ganscha, Oliver T Unke, Klaus-Robert MÃžller, and Stefan Gugler. How simple can you go? an off-the-shelf transformer approach to molecular dynamics. *arXiv preprint arXiv:2503.01431*, 2025.

[60] Filippo Bigi, Marcel F. Langer, and Michele Ceriotti. The dark side of the forces: assessing non-conservative force models for atomistic machine learning. In *Forty-second International Conference on Machine Learning*, 2025.

[61] Johannes Gasteiger, Janek Groß, and Stephan Günnemann. Directional message passing for molecular graphs. *arXiv preprint arXiv:2003.03123*, 2020.

[62] Kai Nordlund, Susi Lehtola, and Gerhard Hobler. Repulsive interatomic potentials calculated at three levels of theory. *Phys. Rev. A*, 111:032818, Mar 2025.

[63] Peter Eastman, Pavan Kumar Behara, David L Dotson, Raimondas Galvelis, John E Herr, Josh T Horton, Yuezhi Mao, John D Chodera, Benjamin P Pritchard, Yuanqing Wang, et al. Spice, a dataset of drug-like molecules and peptides for training machine learning potentials. *Scientific Data*, 10(1):11, 2023.

[64] Peter Eastman, Benjamin P. Pritchard, John D. Chodera, and Thomas E. Markland. Nutmeg and spice: Models and data for biomolecular machine learning. *Journal of Chemical Theory and Computation*, 20(19):8583–8593, 2024.

[65] Keller Jordan, Yuchen Jin, Vlado Boza, Jiacheng You, Franz Cesista, Laker Newhouse, and Jeremy Bernstein. Muon: An optimizer for hidden layers in neural networks, 2024.

[66] K. Anton Feenstra, Berk Hess, and Herman J. C. Berendsen. Improving efficiency of large time-scale molecular dynamics simulations of hydrogen-rich systems. *Journal of Computational Chemistry*, 20(8):786–798, 1999.

[67] Louis Lagardère, Luc-Henri Jolly, Filippo Lipparini, Félix Aviat, Benjamin Stamm, Zhifeng F. Jing, Matthew Harger, Hedieh Torabifard, G. Andrés Cisneros, Michael J. Schnieders, Nohad Gresh, Yvon Maday, Pengyu Y. Ren, Jay W. Ponder, and Jean-Philip Piquemal. Tinker-hp: a massively parallel molecular dynamics package for multiscale simulations of large complex systems with advanced point dipole polarizable force fields. *Chemical Science*, 9:956–972, 2018.

[68] Olivier Adjoua, Louis Lagardère, Luc-Henri Jolly, Arnaud Durocher, Thibaut Very, Isabelle Dupays, Zhi Wang, Théo Jaffrelot Inizan, Frédéric Célerse, Pengyu Ren, Jay W. Ponder, and Jean-Philip Piquemal. Tinker-hp: Accelerating molecular dynamics simulations of large complex systems with advanced point dipole polarizable force fields using gpus and multi-gpu systems. *Journal of Chemical Theory and Computation*, 17(4):2034–2053, 2021.

[69] Joshua A. Rackers, Zhi Wang, Chao Lu, Marie L. Laury, Louis Lagardère, Michael J. Schnieders, Jean-Philip Piquemal, Pengyu Ren, and Jay W. Ponder. Tinker 8: Software tools for molecular design. *Journal of Chemical Theory and Computation*, 14(10):5273–5289, 2018. PMID: 30176213.

[70] Ruhong Zhou, Edward Harder, Huafeng Xu, and B. J. Berne. Efficient multiple time step method for use with ewald and particle mesh ewald for large biomolecular systems. *The Journal of Chemical Physics*, 115(5):2348–2358, 08 2001.